Catheter Configuration for Mapping Micro-Anatomic Reentries Sustaining Atrial Fibrillation

María Termenón-Rivas, Giada S Romitti, Miguel Rodrigo

CoMMLab, Department of Computer Science and Department of Electronic Engineering, Universitat de València, Spain

Abstract

Persistent atrial fibrillation ablation treatment may benefit from multi-electrode mapping (MEM) of extra-pulmonary vein sources, including intramural microanatomic reentries. Optimal MEM configurations to identify micro-reentrant tracks needs to be explored.

Human microanatomic reentrant driver was reproduced in a 3D model (150µm^3 resolution) of atrial tissue with sub-endocardial laterally-insulated myobundle. Unipolar and bipolar electrograms were simulated and local activation time maps were calculated in 876 MEM configurations with variable inter-electrode distances, polarities, orientations, and surface distances.

Action potential simulation of microanatomic reentry showed that the conduction through common reentrant path could be only identifiable by electrodes located < 3 mm from the track. The reentrant track was identifiable in LAT maps from dense unipolar MEM (1 to 6mm spacing) with close surface contact (0.25mm) and for bipolar catheter configurations only when bipoles were aligned to the reentrant path. The reentry was observable >33% on unipolar LAT maps (spacing ≤ 6mm) and on bipolar electrodes with correct orientation (≤ 3mm spacing).

The 3D human AF driver simulation suggested ≤ 3mm inter-electrode and wall contact (<1mm) would be required to map microanatomic reentrant drivers.

1. Introduction

Atrial fibrillation (AF), a prevalent cardiac arrhythmia globally, poses significant morbidity and mortality challenges. Current treatments for AF have limited efficacy and can lead to serious side effects [1]. Primary theories regarding the maintenance mechanisms of persistent AF (perAF) revolve around either multi-wavelets propagating across the atria or localized AF drivers, characterized by areas of rapid, repetitive electrical activity that spreads throughout the atria [2]. Targeted ablation of AF drivers has shown promise in improving treatment efficacy and long-term outcomes compared to conventional pulmonary vein isolation [3]. However, accurately identifying patient-specific AF drivers poses a challenge due to the inadequate visualization of intramural reentrant drivers using surface-only multi-electrode mapping (MEM) [4]. This limitation has resulted in conflicting clinical mapping results and outcomes in AF driver ablation trials [5].

In contrast to MEM, near-infrared optical mapping (NIOM) offers high resolution and subsurface views of electrical conduction, enabling detailed visualization of intramural AF drivers [6]. Recent ex-vivo studies on human atria using transmural NIOM and contrast-enhanced magnetic resonance imaging (CE-MRI) have revealed that AF can be sustained by a limited number of intramural reentry circuits within 3D arrhythmogenic hubs comprised of fibrotically insulated myobundles [7].

However, the optimal MEM configuration needed to identify common reentrant tracks sustaining AF in clinical scenarios are unknown. This computational work simulated an AF episode sustained by a sub-endocardial laterally-insulated myobundle, in which different MEM configurations are tested to identify the micro-reentrant path.

2. Materials and Methods

A 3D model of an atrial slab of tissue (30x30x4mm, 336.241 nodes, 2.017.775 tetrahedral, 150 µm^3 resolution, Fig 1) with sub-endocardial laterally-insulated myobundle of 15x2.5x1.5mm was used to simulate an AF pattern sustained by a micro-anatomical reentry. Each node was simulated as a single atrial cell using the cellular model described by Koivumaki et al. [8] and solved using an adaptive algorithm described in [9]. Electrical remodelling was introduced into the cellular to simulate chronic AF by modifying the following ionic currents: SERCA expression (-16%), PLB to SERC ratio (+18%), SLN to SERCA ratio (-40%), maximal I_{NCX} (+50%), sensitivity of RyR to [Ca2+] SR (+100%), conductance of I_{CaL} (-59%), conductance of Ito (-44%), conductance of I_{Kur} (-22%) and conductance of I_{K1} (+100%) [8]. Heterogeneity in the electrophysiological properties of the micro-reentrant track respect to the atrial myocardium

was introduced as reduced tissue conductivity (-40% respect to atrial wall) in order to simulate slow-path conduction.

Synthetic unipolar EGMs were calculated using cylindrical electrodes (0.5 mm radius, 1 mm length) at different positions and height over the slab of tissue. EGMs were calculated all effective transmembrane contributions over the entire active volume V:

$$u_e(\vec{r_e}, t) = -\frac{1}{4\pi\sigma}\int_V \vec{\nabla}u_m \cdot \left(\frac{\vec{r}}{|\vec{r}|^3}\right) dV$$

where u_e denotes the extracellular potential, $\vec{\nabla}u_m$ denotes the gradient of the transmembrane potential and $\vec{r}$ is the vector from the infinitesimal current density to the recording point $\vec{r_e}$. Computed EGMs were stored for processing at a sampling frequency of 500 Hz.

To evaluate the effect of the electrode distribution and location to properly map this micro-reentry, N=876 electrode configurations were used for mapping. Different inter-electrode distances (1, 3, 6 and 10 mm) were evaluated, as well as 2 different distances to the myo-bundle and atrial wall (0.25 mm and 1 mm). For each case, the LAT map was calculated identifying the activation as the time with maximal negative dV/dt. Additionally, a myobundle-to-wall EGM ratio was created, as the ratio between the amplitude of unipolar EGM shapes corresponding to the myo-bundle activation and to the atrial wall activation, identified by the timing of closer transmembrane potential signal. This allowed to evaluate the relative amplitude of myo-bundle contribution to the EGM conformation, being ratios > 1 cases in which the myo-bundle contribution to the EGM was larger than the atrial wall contribution. Finally, LAT maps with different electrode configuration were used to evaluate the reentry visualization (>75% of cycle), in cases in which at least 4 electrodes in a 2x2 were present.

3. Results

3.1. EGM on Micro-Anatomic Reentries

We wanted to evaluate the ability of different catheter configurations to properly identify cases of AF sustained by micro-anatomic reentries [4]. In this case, the reentrant path is located in a sub-endocardial laterally-insulated myobundle, therefore the 'local' activity to be identified came from a small region, and the effect of 'far' vs 'near' field can be critical for mapping.

Figure 1.A shows the Local Activation Time (LAT) map for the simulation conducted in which a micro-anatomical reentry was sustaining the fibrillatory activity. This reentrant path showed a cycle length of 183 ms, with a conduction velocity of 26 cm/s on the atrial wall and 17 cm/s on the sub-endocardial laterally-insulated myobundle. From panels B and C can be observed as the tissue activated on the atrial wall (B) is larger than the tissue activated on the micro-anatomic path (panel C). Therefore, contributions of the atrial wall activation are expected to be larger on the unipolar EGM (panel D). Here, only unipolar traces from the closer electrode to the micro-reentrant path (0mm) showed a significant depolarization trace during the myobundle activation (AP #3). Unipolar EGM traces from further electrodes (3, 6mm) only showed significant depolarization shapes simultaneously to the atrial wall activation (AP #1).

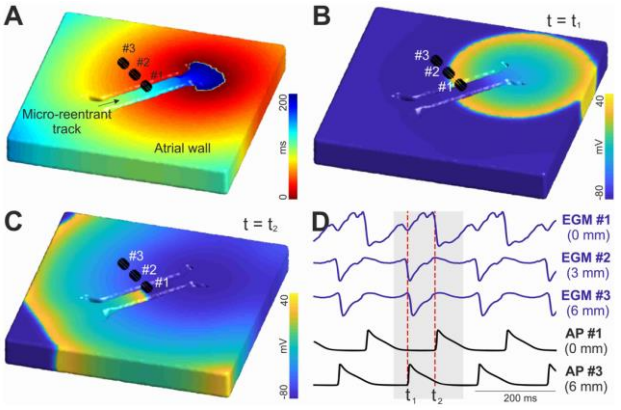

Figure 1. Simulation of micro-anatomical reentry. A) Local Activation Time map. Transmembrane potential for atrial activation (B) and micro-anatomical reentry activation (C). D) EGM traces (blue) for electrodes at 0, 3 and 6 mm from the myobundle (panel A) compared with the transmembrane potentials (black) from their closer points on the atrial wall (AP #1) and on the sub-endocardial laterally-insulated myobundle (AP #3).

3.2. Electrode Configuration for Mapping Micro-Anatomic Reentries

Figure 2 shows the LAT maps obtained for different unipolar catheter configurations, including different electrode spacing (1, 3, 6 and 10 mm) and distances to the atrial wall (0.25 and 1 mm). When the unipolar mapping catheter had good contact with the atrial wall (separation = 0.25mm), the micro-anatomical path was only identifiable for inter-electrode spacings of 1mm and 3mm, and larger spacings reconstructed the LAT maps as a centrifugal propagation. When the mapping catheter had less contact with the atrial wall (separation = 1mm), the micro-anatomical path was identifiable for inter-electrode spacings of 3mm and 6 mm. Even when significant contributions from the myobundle were present (green on myobundle to wall ratio), LAT cannot properly reconstruct the reentrant path.

Same synthetic experiment was conducted for bipolar mapping catheters in Figures 3 and 4. Figure 4 shows the LAT map for bipolar catheters with good contact with the atrial wall (0.25 mm) on two different bipolar

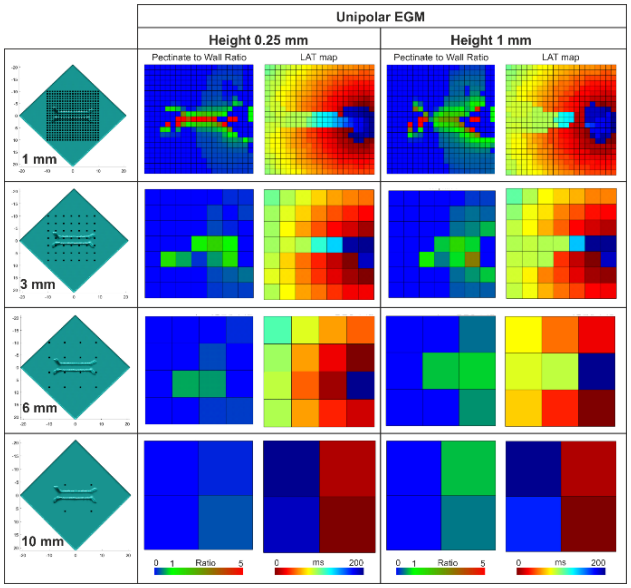

Figure 2. Unipolar mapping of micro-anatomical reentry. The recorded myobundle to wall ratio and LAT map are depicted for each inter-electrode distance (1,3,6 and 10 mm) and distance to the atrial wall (0.25mm and 1mm).

orientations: aligned with the micro-anatomical track (0º) and perpendicular to the micro-anatomical track (90º). Here the micro-anatomical track can be mapped only for the closer inter-electrode distances (1 and 3mm), and only when the bipoles are aligned with the micro-anatomical track. Otherwise, the reentrant track was masked as a focal activation. When the catheter has not good contact (1 mm separation, Fig. 4) the micro-anatomical path was only identified for the closest inter-electrode distance (1mm) and for the aligned orientation.

3.3. Micro-Anatomic Track Identification

In order to systematically evaluate the ability of these different mapping systems to identify the micro-anatomical path, all possible electrode configurations were evaluated, taking into account catheter positions with 1mm displacements from their original position. The presence of the reentrant path was automatically identified as those LAT maps showing at least four contiguous electrodes with activations at 0%, 25%, 50% and 75% of the cycle length with a variation of ± 10%. Table 1 summarizes these findings. In average, unipolar mapping catheters were more likely to detect the micro-reentry compared with bipolar mapping catheters. The chance to identify the micro-anatomical path decreased as the inter-electrode distance increased, and closer distances from the electrode to the wall (0.25 mm) increased the chance to detect the micro-anatomical path. In addition, as expected, bipolar mapping systems only allowed to detect the micro-anatomical path when they had the proper orientation respect to the myobundle.

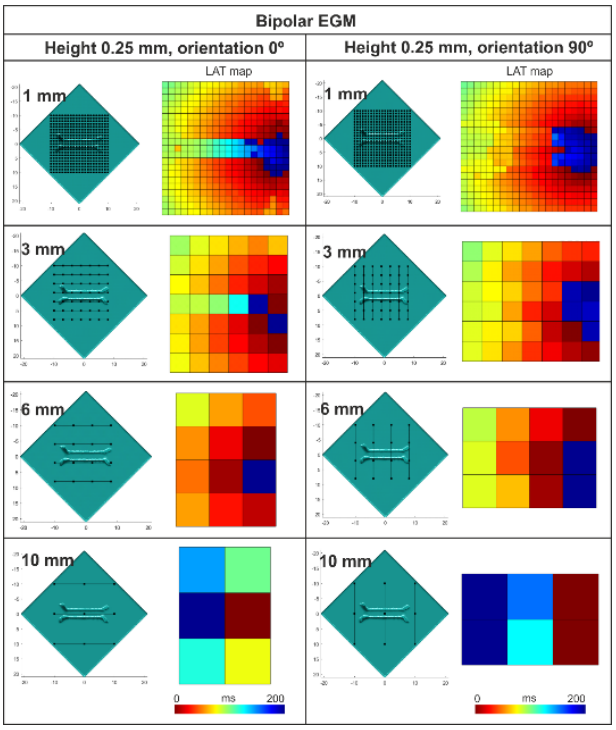

Figure 3. Bipolar mapping of micro-anatomical reentry. LAT map depicted for each inter-electrode distance (1,3,6 and 10 mm) bipolar orientation (0º and 90º), for a separation with the atrial wall of 0.25mm.

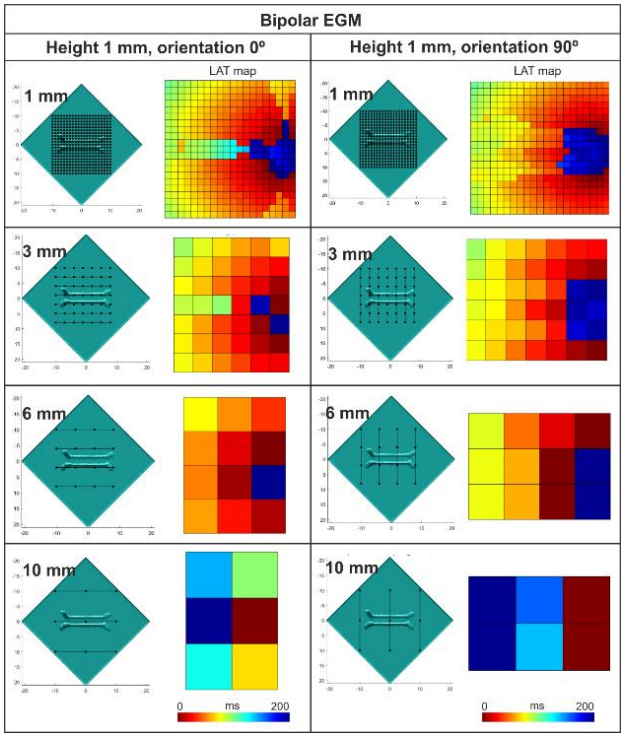

Figure 4. Bipolar mapping of micro-anatomical reentry. LAT map depicted for each inter-electrode distance (1,3,6 and 10 mm) bipolar orientation (0º and 90º), for a separation with the atrial wall of 1mm.

Table 1. Percentage of cases in which the micro-reentry can be identified, depending on the catheter position (micro-reentry identified in LAT map / total cases)

	Unipolar		Bipolar			
	H =	H =	H = 0.25mm		H = 1mm	
Spacing	0.25mm	1mm	O = 0º	O = 90º	O = 0º	O = 90º
1 mm	100% (1/1)	100% (1/1)	100% (1/1)	0% (0/1)	100% (1/1)	0% (0/1)
3 mm	100% (9/9)	89% (8/9)	100% (9/9)	0% (0/9)	44% (4/9)	0% (0/9)
6 mm	47% (17/36)	25% (9/36)	11% (4/36)	0% (0/36)	31% (11/36)	0% (0/36)
10 mm	6% (6/100)	10% (10/100)	0% (0/10)	0% (0/10)	0% (0/10)	0% (0/10)

4. Discussion and Conclusion

This study investigated various MEM configurations, including inter-electrode distances, polarities, orientations, surface distances, and locations relative to the reentrant track, in order to investigate the optimal configuration to identify the micro-reentrant track in typical AF mapping configurations. The study was conducted using a realistic, anisotropic 3D simulation of a sub-endocardial laterally-insulated myobundle sustaining AF by an active reentry. Main results showed that the microanatomic reentry revealed identifiable EGM patterns of the reentrant path, particularly when electrodes were located within 3 mm from the track and with close surface contact. This implied that in multiple electrode configurations (MEM), the reentrant track was identifiable in dense unipolar MEMs (1 to 6mm spacing) only with close surface contact (0.25mm). For bipolar catheter configurations only when bipoles were aligned with the reentrant path, the micro-reentry was identifiable. The reentry was observable >33% of unipolar MEM maps with spacing ≤ 6mm and on bipolar MEMs, only for the correct orientation, when spacing ≤ 3mm spacing.

While this study provides valuable insights into optimal MEM configurations for mapping AF drivers, simulations may not fully capture the complexities of in vivo atrial tissue. Real-world conditions, such as tissue heterogeneity and dynamic changes during AF, could affect the accuracy of mapping results. Moreover, the study focused on a specific cellular model of perAF, potentially limiting the generalizability of the findings. Additionally, the study relied on simulated electrograms rather than actual patient data, which may not fully reflect the variability encountered in clinical practice.

Despite these limitations, the study's findings have significant clinical implications. Optimal MEM configurations may help to improve the accuracy of mapping procedures, leading to more targeted and effective ablation therapies. Close proximity of electrodes to the reentrant path and surface contact are crucial for visualizing micro-anatomic reentrant drivers, so this may imply changes into the current mapping protocols. Incorporating these insights into clinical practice could enhance the success rates of perAF ablation procedures and potentially reduce recurrence rates and complications associated with AF ablation.

Acknowledgments

This work was funded by Generalitat Valenciana Grant AICO/2021/318 (Consolidables 2021) and Grant PID2020-114291RB-I00 funded by MCIN/ 10.13039/501100011033 and by "ERDF A way of making Europe".

References

[1] Verma A, et al. Approaches to Catheter Ablation for Persistent Atrial Fibrillation. N Engl J Med. 2015;372:1812-1822.

[2] Hansen BJ, et al. Maintenance of Atrial Fibrillation: Are Reentrant Drivers With Spatial Stability the Key? Circ Arrhythm Electrophysiol. 2016;9:e004398.

[3] Baykaner T, et al. Clinical Implications of Ablation of Drivers for Atrial Fibrillation: A Systematic Review and Meta-Analysis. Circ Arrhythm Electrophysiol. 2018;11:e006119.

[4] Hansen BJ, et al. Human Atrial Fibrillation Drivers Resolved With Integrated Functional and Structural Imaging to Benefit Clinical Mapping. JACC Clin Electrophysiol. 2018;4:1501-1515.

[5] Miller JM, et al. Clinical Benefit of Ablating Localized Sources for Human Atrial Fibrillation: The Indiana University FIRM Registry. J Am Coll Cardiol. 2017;69:1247-1256.

[6] Walton RD, et al. A Novel Near-Infrared Voltage-Sensitive Dye Reveals the Action Potential Wavefront Orientation at Increased Depths of Cardiac Tissue. Annu Int Conf IEEE Eng Med Biol Soc. 2009;2009:4523-6.

[7] Hansen BJ, et al. Unmasking Arrhythmogenic Hubs of Reentry Driving Persistent Atrial Fibrillation for Patient-Specific Treatment. J Am Heart Assoc. 2020;9:e017789

[8] Koivumäki JT et al., In Silico Screening of the Key Cellular Remodeling Targets in Chronic Atrial Fibrillation," *PLoS computational biology*, vol. 10, no. 5, 2014.

[9] García-Mollá VM et al., Adaptive Step ODE Algorithms for the 3D Simulation of Electric Heart Activity with Graphics Processing Units," *Computers in biology and medicine*, vol. 44, pp. 15-26, 2014.

Address for correspondence:

Miguel Rodrigo Bort.
Av. de l'Universitat s/n, Burjassot 46100, Spain.
miguel.rodrigo@uv.es